

# Broadband passive isolators based on coupled nonlinear resonances

Dimitrios L. Sounas<sup>1</sup>, Jason Soric<sup>1</sup> and Andrea Alù<sup>1,2\*</sup>

**Isolators are devices that transmit waves only in one direction, and are widely used to protect sensitive equipment from reflections and interference. These devices inherently require the breaking of Lorentz reciprocity, which can be achieved with an external bias, such as a magnetic field, that breaks time-reversal symmetry. Alternatively, nonlinear effects can be used, which offer a route to fully passive devices that do not require any form of external bias. However, the nonlinear isolators developed so far have limitations in terms of insertion loss, isolation, bandwidth and isolation intensity range. Here, we show that any isolator formed from one nonlinear resonator suffers from these limitations, and that they can be overcome by combining multiple nonlinear resonators with suitable intensity dispersion. We theoretically show, and then experimentally demonstrate using a microwave circuit, that the combination of one Fano and one Lorentzian nonlinear resonator, and a suitable delay line between them, can provide unitary transmission, infinite isolation, broad bandwidth and broad isolation intensity range. We also show that a larger number of resonators can be used to further increase the isolation intensity range without diminishing the other metrics of the device.**

Non-reciprocal devices such as isolators and circulators are important components in modern microwave and photonic communication systems. The reciprocity breaking that is required with these devices can be accomplished using magnetic bias<sup>1,2</sup>, transistors biased by a direct current<sup>3,4</sup>, or spatiotemporal modulation<sup>5–14</sup>. An alternative approach, which can offer bias-free isolators for applications that do not require simultaneous excitation from opposite directions, such as in pulsed lasers, involves using optical nonlinearities<sup>15–33</sup>. Most commonly this is based on resonant structures loaded with third-order nonlinear materials<sup>16–32</sup>, that is, materials with permittivity  $\epsilon = \epsilon_{\text{lin}} + \chi^{(3)} |\mathbf{E}|^2$ , where  $\epsilon_{\text{lin}}$  is the linear permittivity,  $\chi^{(3)}$  the nonlinear susceptibility and  $\mathbf{E}$  the electric field intensity. This type of nonlinearity is responsible for shifting the resonance frequency as a function of the input intensity. If the resonator is asymmetric from opposite sides, the frequency shift is different from opposite excitations, resulting in asymmetric transmission and a non-reciprocal response.

In this context, Fano resonators are particularly well suited for the design of nonlinear isolators<sup>27–32</sup> because of their sharp frequency response, which results in a fast transition from low to high transmission as the input intensity exceeds a certain threshold. Breaking spatial symmetry in Fano resonators leads to an intensity scaling of the response of the resonator when the propagation direction is reversed, thus producing isolation. At any frequency, if the propagation direction is reversed, the intensity that leads to a certain transmission is scaled by the linear asymmetry factor of the resonator,  $\kappa_{\text{lin}}$ , defined as the ratio of the induced field intensity for excitation from opposite sides in the linear (low-intensity) regime. Based on this property, the isolation intensity range (IIR) can be defined as the ratio of input intensities from opposite propagation directions that lead to the same transmission coefficient. A large IIR corresponds to an isolator that exhibits significant isolation over a large range of input intensities. Because  $\text{IIR} = \kappa_{\text{lin}}$ , it is possible to design an isolator with a broad intensity response by increasing the asymmetry of the structure.

Fano nonlinear isolators are subject to a fundamental trade-off between transmission in the forward (allowed) direction ( $T_{\text{fw}}$ ) and IIR (D. L. Sounas et al., manuscript in preparation). In particular, a large  $\kappa_{\text{lin}}$  implies a large separation between transmission from opposite sides, and therefore a large IIR. We have, however, previously shown<sup>34</sup> that time-reversal symmetry imposes the following restriction between  $T_{\text{fw}}$  and  $\kappa_{\text{lin}}$ :

$$T_{\text{fw}} \leq \frac{4\kappa_{\text{lin}}}{(\kappa_{\text{lin}} + 1)^2} \quad (1)$$

Equation (1) shows that  $T_{\text{fw}}$  decreases as  $\kappa_{\text{lin}}$  increases, implying that either we select a narrowband and narrow intensity range to achieve low insertion loss, or we sacrifice forward transmission to operate over a broad range of input intensities and bandwidths. In the ideal case of unitary transmission and zero insertion loss ( $T_{\text{fw}} = 1$ ),  $\kappa_{\text{lin}} = 1$  and the resonator exhibits the same response from opposite sides, becoming reciprocal. In addition to the bound between IIR and  $T_{\text{fw}}$ , equation (1) implies a similar bound between the isolation bandwidth and  $T_{\text{fw}}$ . Considering that the operation of a Fano nonlinear isolator is based on an asymmetric shift of its resonance frequency when excited from opposite sides, the overall isolation bandwidth is proportional to the difference between the resonant frequencies of the resonator for excitation from opposite sides, determined by  $\kappa_{\text{lin}}$ . Therefore, a large isolation bandwidth requires a large  $\kappa_{\text{lin}}$ ; however, according to equation (1), this comes at the expense of a reduced  $T_{\text{fw}}$ .

In this Article we show that these limitations of Fano isolators apply to any isolator with a single nonlinear resonator, and that they can be broken by using multiple nonlinear resonators. We then show that we can efficiently control the non-reciprocal response of the isolator, including forward transmission, isolation and IIR, by appropriately selecting the number and characteristics of the

<sup>1</sup>Department of Electrical and Computer Engineering, The University of Texas at Austin, Austin, TX, USA. <sup>2</sup>Advanced Science Research Center, City University of New York, New York, NY, USA. \*e-mail: [aalu@gc.cuny.edu](mailto:aalu@gc.cuny.edu)

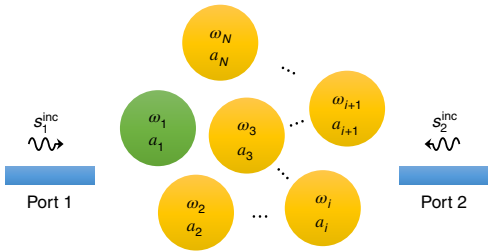


**Fig. 1 | Nonlinear isolator based on a single nonlinear resonator.** In addition to the nonlinear resonator (green), an arbitrary number of linear resonators (yellow) can be connected in an arbitrary way with one another.

resonators. Finally, we provide an experimental validation of these concepts at microwave frequencies.

### Limitations of isolators with a single nonlinear resonator

Consider a system of  $N$  resonators in which only one (resonator 1) is nonlinear and the rest are linear (Fig. 1). By using coupled-mode theory (see Methods), the resonant amplitude in the nonlinear resonator (resonator 1) is given by

$$a_1 = \frac{a_{1,\text{lin}}^{(1)}}{1 - iG_{11}\Delta\omega_1} s_1^{\text{inc}} + \frac{a_{1,\text{lin}}^{(2)}}{1 - iG_{11}\Delta\omega_1} s_2^{\text{inc}} \quad (2)$$

where  $s_i^{\text{inc}}$  is the incident signal from the  $i$ th port;  $a_1^{(i)}$  is the resonant amplitude in resonator 1 in the linear regime for excitation with a signal of unitary amplitude from the  $i$ th port;  $\Delta\omega_1$  is the shift of the resonance frequency of resonator 1 due to the nonlinear effect, given by  $\Delta\omega_1 = -\omega_{1,\text{lin}} |a_1|^2 / |a_{10}|^2$ , where  $\omega_{1,\text{lin}}$  is the resonance frequency of resonator 1 in the linear regime and  $|a_{10}|^2$  is a characteristic quantity of the resonator with units of energy; and  $G_{11}$  is a characteristic parameter of the system that depends only on its linear properties. From equation (2) and  $\Delta\omega_1 = -\omega_{1,\text{lin}} |a_1|^2 / |a_{10}|^2$  it follows that

$$\frac{\Delta\omega_1^{(2)}}{\Delta\omega_1^{(1)}} \left| \frac{1 - iG_{11}\Delta\omega_1^{(2)}}{1 - iG_{11}\Delta\omega_1^{(1)}} \right|^2 = \kappa_{\text{lin}} \frac{|s_2^{\text{inc}}|^2}{|s_1^{\text{inc}}|^2} \quad (3)$$

where  $\Delta\omega_1^{(i)}$  is the resonance frequency shift of resonator 1 for excitation from the  $i$ th port with a signal  $s_i^{\text{inc}}$ , and  $\kappa_{\text{lin}} = |a_{1,\text{lin}}^{(2)}|^2 / |a_{1,\text{lin}}^{(1)}|^2$  is the linear asymmetry parameter in resonator 1. Equation (3) shows that the resonance frequency variation from port 2 is equal to the one from port 1, if the input power from port 1 is  $\kappa_{\text{lin}}$  times larger than that from port 2. Given that the same frequency variation from different ports implies the same transmission coefficient, we deduce that transmission from different ports is the same if the input power from port 1 is  $\kappa_{\text{lin}}$  times larger than from port 2, as in nonlinear Fano resonators. Then, from the definition of IIR it follows that  $\text{IIR} = \kappa_{\text{lin}}$ .

Assume now that the system is excited from port 1 with signal  $s_1^{\text{inc}}$ . From equation (2) we find

$$a_1 = \frac{a_{1,\text{lin}}^{(1)}}{1 - iG_{11}\Delta\omega_1} s_1^{\text{inc}} \quad (4)$$

Furthermore, assuming that the nonlinear reflection and transmission coefficients for this particular excitation intensity are  $r_{\text{NL}}$

and  $t_{\text{NL}}$ , respectively, the output signals at ports 1 and 2 are  $r_{\text{NL}} s_1^{\text{inc}}$  and  $t_{\text{NL}} s_1^{\text{inc}}$ , respectively. Performing a time-reversal operation, we consider a scenario where the system is excited with signals  $r_{\text{NL}}^* (s_1^{\text{inc}})^*$  and  $t_{\text{NL}}^* (s_1^{\text{inc}})^*$  from ports 1 and 2, respectively, and the resonant amplitude in resonator 1 is  $a_1^*$ , with the asterisk denoting complex conjugation. Because  $\Delta\omega_1$  depends only on  $|a_1|^2$ , it is the same as in the original excitation scenario (it is not affected by the time-reversal operation), allowing equation (2) to be applied in the time-reversed scenario as

$$a_1^* = \frac{a_{1,\text{lin}}^{(1)}}{1 - iG_{11}\Delta\omega_1} r_{\text{NL}}^* (s_1^{\text{inc}})^* + \frac{a_{1,\text{lin}}^{(2)}}{1 - iG_{11}\Delta\omega_1} t_{\text{NL}}^* (s_1^{\text{inc}})^* \quad (5)$$

Inserting equation (4) into equation (5) yields

$$\begin{aligned} & \frac{a_{1,\text{lin}}^{(1)*}}{1 + iG_{11}^* \Delta\omega_1} (s_1^{\text{inc}})^* \\ &= \frac{a_{1,\text{lin}}^{(1)}}{1 - iG_{11}\Delta\omega_1} r_{\text{NL}}^* (s_1^{\text{inc}})^* + \frac{a_{1,\text{lin}}^{(2)}}{1 - iG_{11}\Delta\omega_1} t_{\text{NL}}^* (s_1^{\text{inc}})^* \end{aligned} \quad (6)$$

Equation (6) can also be written as  $\frac{1 - iG_{11}\Delta\omega_1}{1 + iG_{11}^* \Delta\omega_1} a_{1,\text{lin}}^{(1)*} = r_{\text{NL}}^* a_{1,\text{lin}}^{(1)} + t_{\text{NL}}^* a_{1,\text{lin}}^{(2)}$ , which, apart from the factor  $\frac{1 - iG_{11}\Delta\omega_1}{1 + iG_{11}^* \Delta\omega_1}$ , is the same equation imposed by time-reversal symmetry on linear systems<sup>34</sup>. Observing that  $\frac{1 - iG_{11}\Delta\omega_1}{1 + iG_{11}^* \Delta\omega_1}$  has a unitary amplitude, it is possible to show that the system in Fig. 1 is still subject to equation (1). This, combined with the fact that  $\text{IIR} = \kappa_{\text{lin}}$ , shows that, despite the arbitrary nature of the network in Fig. 1, systems with a single nonlinear resonator are subject to the same limitations as Fano resonators in terms of trade-off between IIR and forward insertion loss.

### Broadband isolators with multiple nonlinear resonators

To overcome equation (1) and realize broadband, highly efficient passive isolators, we need to consider, at a minimum, two coupled nonlinear resonators. This idea was explored in ref. <sup>35</sup> for a system of two Lorentzian resonators, but here we show that it is possible to achieve full control over forward transmission, isolation, bandwidth and IIR by combining two or more nonlinear Lorentzian and Fano resonators, yielding unitary forward transmission, infinite isolation, broad bandwidth and broad intensity range. Consider, for instance, a system consisting of a nonlinear Lorentzian resonator and a nonlinear Fano resonator (Fig. 2). Due to the nonlinearity, transmission through each of the resonators changes with input intensity up to a maximum value determined by equation (1), which for symmetric resonators is equal to unity. We designed the resonators to independently exhibit a unitary transmission peak for the same input intensity of interest (Fig. 2a). As expected, when the resonators are cascaded, they will also exhibit unitary transmission at the same input intensity (Fig. 2b). For any other input intensity, the Lorentzian and Fano resonators exhibit non-unitary transmission, leading to an asymmetric system with non-zero IIR, despite the unitary transmission in the forward direction, thereby breaking equation (1).

To better understand the mechanism that produces asymmetry in the system in Fig. 2a, we studied the response of the system when excited from opposite directions with signals of increasing intensity. Consider first exciting the system from the side of the Fano resonator. For low intensities the input signal is almost totally reflected by the Fano resonator, without having the chance to interact with the Lorentzian resonator. On the other hand, when the intensity is high enough for the signal to be transmitted through the Fano resonator

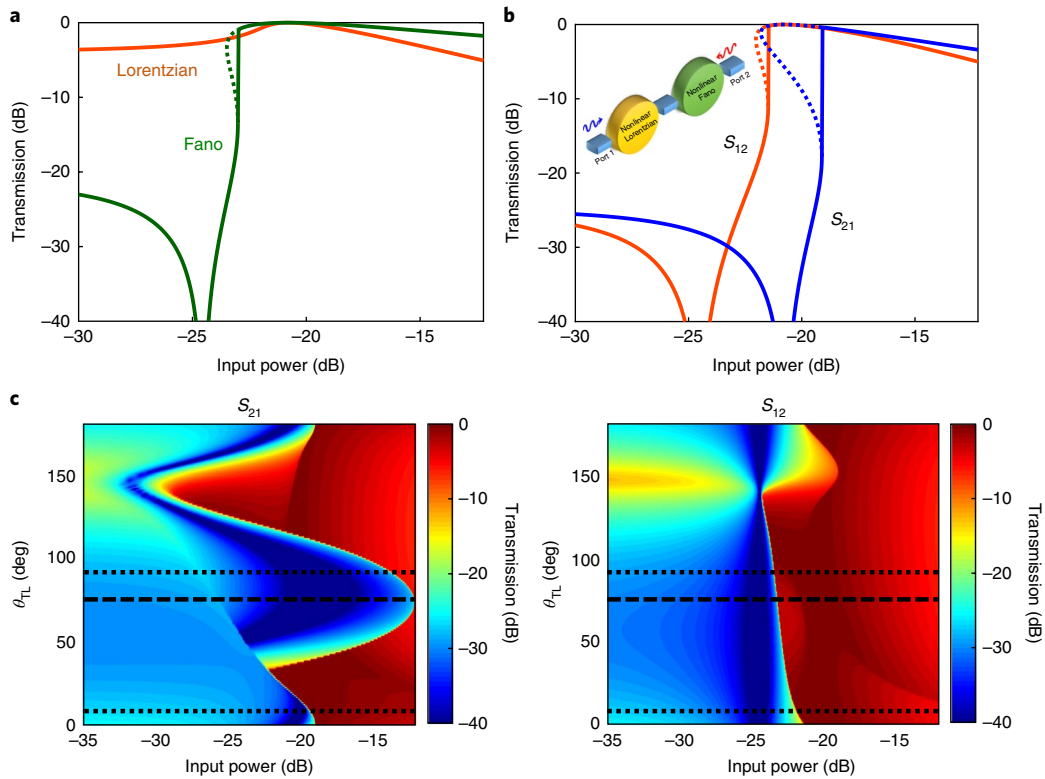


**Fig. 2 | Nonlinear isolator based on a nonlinear Lorentzian resonator and a nonlinear Fano resonator.** **a**, Nonlinear response for the two resonators when they are separated from each other. **b**, Nonlinear response when the resonators are back to back. Solid lines show the response for increasing input intensity.  $S_{21}$  is the transmission coefficient from port 1 to 2.  $S_{12}$  is the transmission coefficient from port 2 to 1. The dotted lines in **a** and **b** correspond to either unstable branches or branches that can be accessed only for decreasing input intensities. **c**, Nonlinear response versus input intensity and the electrical length  $\theta_{TL}$  of a delay line between the resonators. Dotted lines correspond to systems that exhibit peak transmission from one direction and zero transmission from the other for the same intensity. The dashed line corresponds to a system with maximum IIR. In all cases, the intensity is presented on a normalized dB scale. Details of the modelling of the resonators and their parameters are provided in the Methods and Supplementary Table 1, respectively.

and subsequently interact with the Lorentzian resonator, reflection from the Lorentzian resonator is not significant enough to perturb the operation point of the Fano resonator. As a result, for excitation from the side of the Fano resonator, the response of the system is similar to that of the Fano resonator alone. The situation is different when the system is excited from the side of the Lorentzian resonator. In this case, and for excitation of low intensity, the transmitted signal through the Lorentzian resonator is almost perfectly reflected by the Fano resonator and then partially reflected at the inner side of the Lorentzian resonator. As a result, the incident power that interacts with the Fano resonator is given by

$$|s_F^{inc}|^2 = \frac{1-R_L}{1+R_L-2\sqrt{R_L}\cos\varphi} |s_1^{inc}|^2 \quad (7)$$

where  $|s_1^{inc}|^2$  is the incident power at port 1,  $|s_F^{inc}|^2$  is the incident power at the inner side of the Fano resonator,  $R_L$  is the reflection coefficient from the Lorentzian resonator, and  $\varphi$  is the sum of the reflection phases from the Lorentzian and Fano resonators. Depending on the values of  $R_L$  and  $\varphi$ ,  $|s_F^{inc}|^2$  can be larger or smaller than  $|s_1^{inc}|^2$ , shifting the transmission transition threshold to lower or higher values compared to the Fano resonator. For example, in Fig. 2b the transition threshold is slightly shifted to higher values. If we now consider a delay line between the resonators, we can control  $\varphi$  and in turn the IIR of the system. This can be clearly seen in Fig. 2c, which presents the system's response versus the input intensity and transmission line electrical length. A particularly interesting case

occurs when the transmission zero is pushed to very large intensities, as shown with the dashed lines in Fig. 2c, resulting in very large isolation (larger than 30 dB) and a broad range of input intensities (larger than 10 dB). Another interesting scenario is observed when the transmission zero from one direction occurs at the same intensity as the transmission peak from the other direction (dotted lines in Fig. 2c), leading to a nonlinear isolator with unitary transmission and infinite isolation at the same intensity. Such isolators largely overcome the limitations of nonlinear isolators presented so far in the literature, as well as the bound in equation (1). It is important to note that when the transmission is unitary from one direction it can also become unitary from the opposite direction as a consequence of time-reversal symmetry. However, for the backward direction, the point of unitary transmission belongs to the upper branch of a bistable region, and it is therefore inaccessible as we increase the input intensity.

A problem with the system described above is that forward transmission is close to unity only over a narrow range of input intensities, which, given the frequency dispersion of the resonators, translates into equally narrow bandwidths of operation, limiting the efficiency of the isolator under excitation with pulses. For example, for the system in Fig. 2c, the intensity range over which  $T_{fw}$  is larger than  $-1$  dB assuming the largest possible IIR (dashed line in Fig. 2c) is 3.6 dB. Although it is impossible to make a nonlinear isolator that exhibits unitary transmission for any input intensity—there will always be a range of intensities close to the linear regime where forward transmission is small—it is possible to extend the intensity range where transmission is above a certain level by

combining a larger number of resonators. As an example, here we study a system consisting of two pairs of Lorentzian and Fano resonators (Fig. 3). The main idea is to design each pair to exhibit quasi-unitary transmission over a desired range of input intensities, so that when the two pairs are combined they also exhibit quasi-unitary transmission over the same intensity range. To this end we selected each pair to consist of two identical resonators. It is evident that the pair of resonators exhibits unitary transmission at the same intensity as its constituent resonators. However, adding a delay line between the resonators allows us to obtain unitary transmission at another input intensity, which can be efficiently controlled over a large range of values by changing the value of the phase delay (Fig. 3a,b). Furthermore, by connecting the two pairs with another delay line, we can control the transmission transition intensity associated with the Fano response as in the system of individual Lorentzian and Fano resonators, allowing a system to be obtained that exhibits very large isolation, large IIR and at the same time high quasi-flat forward transmission over a large range of input intensities. Figure 3c shows the response of such a system based on the same Fano resonator as in Fig. 2. We can see that the range of input intensities where forward transmission is larger than  $-1$  dB has increased from 3.6 dB to 6 dB. This approach can be further extended to arrays of nonlinear resonators, thereby opening and controlling continuous broad bandwidths of nonlinear isolation with large flexibility.

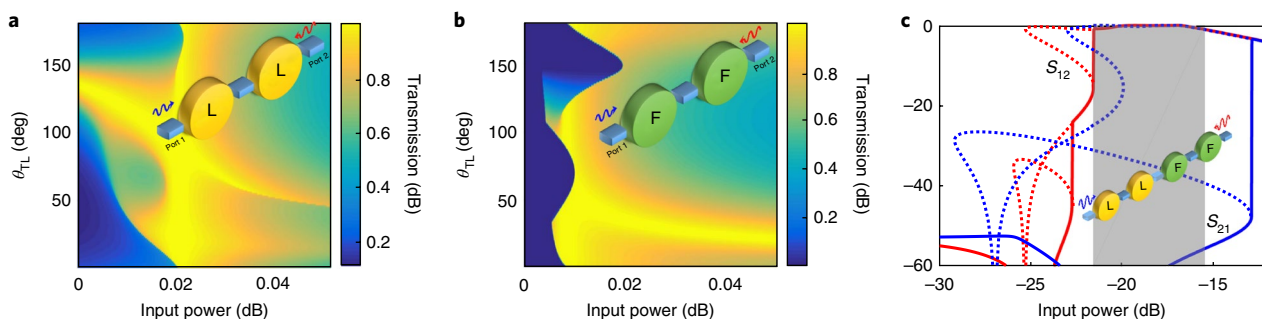
### Experimental demonstration at microwave frequencies

To prove the feasibility of the theoretical results presented above, we experimentally realized the system of Fig. 2, consisting of a cascaded Lorentzian resonator and Fano resonator, using lumped-circuit elements over a printed circuit board (PCB) (Fig. 4a). For the Lorentzian resonator we used a parallel  $LC$  network connected to ground, which exhibits a symmetric response around its resonance frequency. To be able to control the linewidth of the resonator, the  $LC$  resonator was placed between two identical capacitors. For the Fano resonator we used a parallel combination of a series  $LC$  resonator and a capacitor, both connected to ground. At its resonance, the  $LC$  network is a short circuit, resulting in zero transmission. On the other hand, at the resonance of the loop consisting of the  $LC$  network and the shunt capacitor, the effective impedance to ground is infinite, and transmission is unitary. The existence of both zero and unitary transmission is a signature of a Fano response. All the properties of this Fano response, including the positions of the zero, peak and background transmission, can be controlled through the design choice of the circuit elements. We also added a short transmission line between the resonators to enable control of the position of the transmission zero, as described in the section

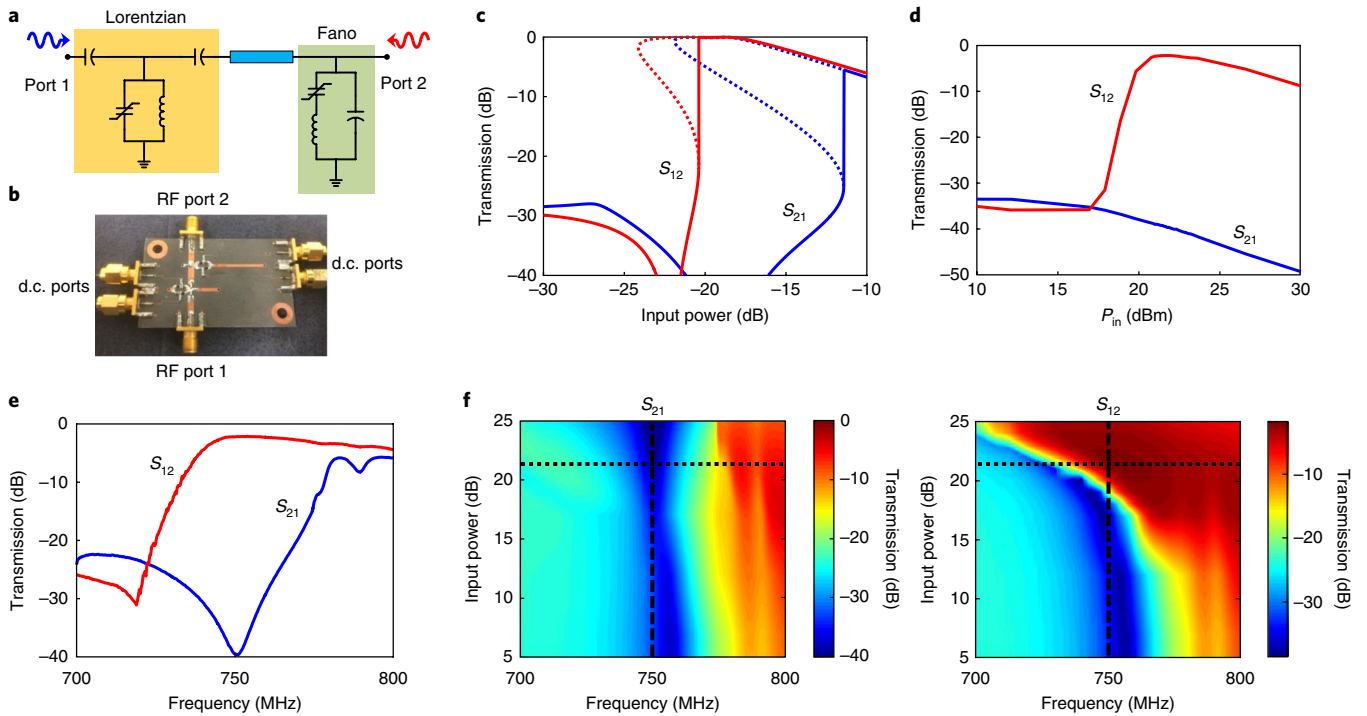
'Broadband isolators with multiple nonlinear resonators'. The resonators were realized using varactors, which introduce nonlinearity into the system. In particular, to achieve a response similar to an instantaneous Kerr effect, for each nonlinear capacitor we used a parallel combination of identical varactors with opposite polarity, as explained in the Methods. A photograph of the fabricated circuit is presented in Fig. 4b.

Figure 4c presents the simulated response of the circuit, assuming ideal (lossless) components. All the parameters in the simulation and experiment are provided in the Methods. The transmission line length was selected to align the transmission zero from one direction with the transmission peak from the other one and yield infinite isolation. We can see that, for a certain intensity, the structure exhibits unitary transmission from one direction and zero transmission from the other, and yields an overall large IIR. By tuning the transmission line length, we can push the transmission zero to higher intensities and realize an isolator with large isolation over an even broader intensity range, which may be interesting for several applications. Figure 4d presents measurement results for transmission from opposite sides versus the input intensity  $P_{in}$  for the realized device. The excitation frequency is slightly different from that found in simulations due to the parasitic effects that exist in any PCB circuit. The peak transmission is  $-2$  dB (0.63 on a linear scale) with an IIR range larger than 12 dB. Notice that the measured IIR is even larger than in simulations, which we attribute to higher-order nonlinear effects that were not considered in our model. The transmission is non-unitary due to losses of the components. However, even with this loss, the transmission is much larger than the maximum transmission predicted by equation (1) for an ideal lossless system based on a single nonlinear resonator and the same IIR. In particular, for a system based on a single nonlinear resonator, an IIR of 12 dB corresponds to a maximum peak transmission of  $-6.5$  dB (0.22 in linear scale) allowed by equation (1), assuming zero loss. In reality, this value would be even smaller due to the losses of all realistic components. We yield significantly larger transmission, which may be increased to unitary with better fabrication. In addition to the large transmission and broad IIR, the circuit in Fig. 4 exhibits very large isolation, larger than 30 dB over the entire measured IIR.

Figure 4e presents measurement results for transmission versus frequency at an input intensity of 21 dBm, which corresponds to the maximum forward transmission in Fig. 4d. The device follows a Fano dispersion, with transmission changing from low to high values as the input frequency is swept across the resonance frequency of the Fano resonator. Due to the nonlinearity and asymmetry of the structure, the resonance frequency of the Fano resonator, and consequently the transition frequency, is different



**Fig. 3 | Nonlinear isolator based on multiple nonlinear resonators.** **a**, Transmission through a pair of Lorentzian resonators (L) versus the input intensity and phase delay between the resonators. **b**, As in **a** for the pair of Fano resonators (F). **c**, Response of the combined system.  $S_{21}$ , transmission from port 1 to 2.  $S_{12}$ , transmission from port 2 to 1. The solid lines show the response for increasing input intensity. The dotted lines correspond to either unstable branches or branches that can be accessed only for decreasing input intensities. The shaded region corresponds to input intensities for which transmission in the backward direction  $S_{12}$  is larger than  $-1$  dB. Details of modelling of the resonators and their parameters are provided in the Methods and Supplementary Table 2, respectively.



**Fig. 4 | Microwave realization of a Lorentzian-Fano nonlinear isolator.** **a**, Schematic of the circuit. The values of the circuit elements are provided in Supplementary Table 3. **b**, Photograph of the fabricated prototype. The d.c. ports are used to bias the varactors, which are used to implement the nonlinear capacitors. **c**, Numerical transmission results, assuming ideal elements (zero loss), at 900 MHz. The transmission line length was selected to achieve alignment of the transmission peak from one direction with the transmission zero from the other. The intensity is presented on a dB scale normalized with respect to  $V_0^2/(2Z_0)$ , where  $V_0$  is the characteristic voltage of the varactor defined in Methods and  $Z_0$  is the transmission line impedance. The dotted lines correspond to either unstable branches or branches that can be accessed only for decreasing input intensities. **d**, Experimental results for transmission versus input intensity at 750 MHz. **e**, Experimental results for transmission versus frequency for an input power of 21 dBm. **f**, Experimental results for the S-parameters versus frequency and input intensity. Dashed lines correspond to the operating frequency in **d**. Dotted lines correspond to the input power in **e**.

for opposite excitation directions. For a simple Fano isolator this frequency shift is determined by the asymmetry factor  $\kappa_{\text{lin}}$  and, as a result, it is subject to the bound in equation (1). A larger forward transmission necessarily leads to a narrower isolation bandwidth, and in the case of unitary forward transmission the isolation bandwidth would completely vanish. Figure 4e, on the other hand, shows that our isolator can achieve a large bandwidth (50 MHz in Fig. 3e), and at the same time a large forward transmission. Finally, Fig. 4f presents experimental results for the response of the system versus both input intensity and frequency. For excitation from port 1, the transmission is smaller than  $-25$  dB for any input intensity if the frequency is smaller than 770 MHz, essentially following the linear response of the system. On the other hand, for excitation from the opposite side, there is always an input intensity at which the transmission experiences a fast transition from low to high values. Beyond this intensity, the structure operates as an isolator with large isolation and low loss. These measurements confirm that the proposed isolator not only has a broad IIR, but also a broad bandwidth of operation.

**Conclusions**

We have reported an approach for the design of passive nonlinear isolators with full control over their forward transmission, isolation and isolation intensity range, based on the combination of nonlinear Lorentzian and Fano resonators separated by suitably designed delay lines. We have also validated our general theoretical analysis with an experimental demonstration at microwave frequencies. Increasing the number of resonators offers more flexibility in controlling transmission and isolation over a given intensity range, similar

to the frequency response of linear filters based on multiple linear resonators<sup>36</sup>. Given that in these systems time-reversal symmetry is broken by the signal itself, due to nonlinearity, isolation is not necessarily expected when the system is excited at the same time from opposite ports<sup>33</sup>. In this sense, our results shed light on the limitations of nonlinear isolators and clarify the conditions for their optimum design and operation for pulsed signals. The design flexibility introduced by the use of multiple nonlinear resonators and delay lines with suitable dispersion, exploited here to realize broadband nonlinear isolators with large isolation and low insertion loss, may also enable countermeasures to reduce or eliminate the effect of interference from signals impinging from opposite ports.

**Methods**

**Isolators with a single nonlinear resonator.** Here, we generally prove equation (2) for nonlinear isolators with a single nonlinear resonator and an arbitrary number of linear resonators, as in Fig. 1, where resonator 1 is assumed to be nonlinear. The resonant frequency of the nonlinear resonator is given by

$$\omega_1 = \omega_{1,\text{lin}} \left( 1 - \frac{|a_1|^2}{|a_{10}|^2} \right) \tag{8}$$

where  $\omega_{1,\text{lin}}$  is the resonance frequency in the linear regime,  $|a_1|^2$  is the stored energy in the resonator and  $|a_{10}|^2$  is a characteristic quantity of the resonator with units of energy<sup>37</sup>. Equation (8) describes the response of a resonator with instantaneous Kerr-type nonlinearity. All the other resonators have constant (intensity-independent) resonant frequencies  $\omega_j$ , with  $j = 2, \dots, N$ . Furthermore, because the nonlinear effect is only a perturbation of the material properties of resonator 1, we assume that it does not affect the coupling between the resonators and their decay rates.

The system can be efficiently described through coupled-mode theory (CMT) as

$$\frac{d\mathbf{a}}{dt} = (i\Omega - \Gamma)\mathbf{a} + \mathbf{k}_1 s_1^{\text{inc}} + \mathbf{k}_2 s_2^{\text{inc}} \quad (9)$$

where  $\mathbf{a} = [a_1, a_2, \dots]^T$  is the modal vector,  $\Omega$  is the system's frequency matrix,  $\Gamma$  is the system's decay matrix,  $s_j^+$  is the incident signal from the  $j$ th port,  $\mathbf{k}_j$  is the coupling vector between the system and the  $j$ th port, and  $s_j^{\text{inc}}$  is the incident signal from the  $j$ th port<sup>38</sup>. The diagonal components of  $\Omega$  are the resonance frequencies of the resonators, and the off-diagonal components provide the coupling between the resonators. Similar considerations also hold for  $\Gamma$ . For  $\mathbf{k}_j$ , the  $n$ th component describes the coupling between the  $n$ th resonator and the  $j$ th port. From the assumptions mentioned in the previous paragraph, nonlinearity affects only the 11 component of  $\Omega$ , which is equal to  $\omega_1$ . In particular,  $\omega_1 = \omega_{1,\text{lin}} + \Delta\omega_1$ , where  $\Delta\omega_1 = -\omega_{1,\text{lin}} |a_1|^2 / |a_{10}|^2$ . Then, it follows

$$\Omega = \Omega_{\text{lin}} + \Delta\Omega \quad (10)$$

where  $\Omega_{\text{lin}}$  is the frequency matrix in the linear regime and

$$\Delta\Omega = \begin{bmatrix} \Delta\omega_1 & 0 & \dots \\ 0 & 0 & \dots \\ \vdots & \vdots & \ddots \end{bmatrix} \quad (11)$$

If the system is excited with harmonic signals with frequency  $\omega$ , equation (9) can be written as

$$H\mathbf{a} = \mathbf{k}_1 s_1^{\text{inc}} + \mathbf{k}_2 s_2^{\text{inc}} \quad (12)$$

where  $H = i(\omega I - \Omega) + \Gamma$ , where  $I$  is the identity matrix. Inserting equation (10) into equation (11) yields

$$H_{\text{lin}}\mathbf{a} = i\Delta\Omega\mathbf{a} + \mathbf{k}_1 s_1^{\text{inc}} + \mathbf{k}_2 s_2^{\text{inc}} \quad (13)$$

where  $H_{\text{lin}} = i(\omega I - \Omega_{\text{lin}}) + \Gamma$ . Substituting  $\Delta\Omega$  from equation (11) into equation (13) yields

$$H_{\text{lin}}\mathbf{a} = i\Delta\omega_1 a_1 \mathbf{e}_1 + \mathbf{k}_1 s_1^{\text{inc}} + \mathbf{k}_2 s_2^{\text{inc}} \quad (14)$$

where  $\mathbf{e}_1 = [1 \ 0 \ 0 \ \dots \ 0]^T$ . Multiplying equation (14) with  $H_{\text{lin}}^{-1}$  and taking the first line of the resulting matrix equation gives

$$a_1 = i\Delta\omega_1 (H_{\text{lin}}^{-1})_{11} a_1 + (H_{\text{lin}}^{-1}\mathbf{k}_1)_1 s_1^{\text{inc}} + (H_{\text{lin}}^{-1}\mathbf{k}_2)_1 s_2^{\text{inc}} \quad (15)$$

where  $(H_{\text{lin}}^{-1})_{11}$  is the 11 component of  $H_{\text{lin}}^{-1}$ , and  $(H_{\text{lin}}^{-1}\mathbf{k}_1)_1$  is the first component of  $H_{\text{lin}}^{-1}\mathbf{k}_1$ . Note that  $(H_{\text{lin}}^{-1}\mathbf{k}_1)_1$  is the mode amplitude in resonator 1 in the linear regime for excitation from the  $j$ th port with a signal of unitary amplitude. We will use the notation  $a_{1,\text{lin}}^{(j)}$  for this quantity. Then, solving equation (15) for  $a_1$  gives

$$a_1 = \frac{a_{1,\text{lin}}^{(1)}}{1 - i\Delta\omega_1 (H_{\text{lin}}^{-1})_{11}} s_1^{\text{inc}} + \frac{a_{2,\text{lin}}^{(2)}}{1 - i\Delta\omega_1 (H_{\text{lin}}^{-1})_{11}} s_2^{\text{inc}} \quad (16)$$

By defining  $G_{11} = (H_{\text{lin}}^{-1})_{11}$ , we end up with equation (2).

**CMT for Lorentzian and Fano resonators.** Here, we provide details about the CMT models that were used to obtain the theoretical results in Figs. 2 and 3. A symmetric Fano resonator with two ports is described through the equations

$$\frac{da}{dt} = (i\omega_0 - \gamma)a + \kappa(s_1^{\text{inc}} + s_2^{\text{inc}}) \quad (17)$$

and

$$\begin{aligned} s_1^{\text{ref}} &= r s_1^{\text{inc}} + t s_2^{\text{inc}} + \kappa a \\ s_2^{\text{ref}} &= r s_2^{\text{inc}} + t s_1^{\text{inc}} + \kappa a \end{aligned} \quad (18)$$

where  $a$  is the resonant amplitude,  $\omega_0$  is the resonance frequency,  $\gamma$  is the decay rate,  $\kappa$  is the coupling coefficient from either port,  $s_i^{\text{inc}}$  is the incident signal at the  $i$ th port,  $s_i^{\text{ref}}$  is the reflected signal at the  $i$ th port, and  $r$  and  $t$  are the background reflection and transmission coefficients between the ports, that is, the reflection and transmission coefficients for frequencies far from  $\omega_0$ . Power conservation leads to the following relations:

$$\begin{aligned} |r|^2 + |t|^2 &= 1 \\ \text{Re}\{rt^*\} &= 0 \\ \kappa &= \sqrt{-\gamma(r+t)} \end{aligned} \quad (19)$$

The case of Lorentzian resonators is recovered for  $t=0$ . Equations (19) provide freedom in the selection of the phase of  $r$  or  $t$ , which physically corresponds to shifting the reference plane for the ports. In the results presented in the main text, we have assumed  $\arg\{r\} = 0$  and  $\arg\{t\} = \pi/2$ . If the resonator is nonlinear,  $\omega_0$  depends on the stored energy as

$$\omega_0 = \omega_{0,\text{lin}} \left( 1 - \frac{|a|^2}{|a_0|^2} \right) \quad (20)$$

where  $\omega_{0,\text{lin}}$  is the resonance frequency in the linear regime, and  $|a_0|^2$  is a characteristic quantity of the resonator with units of energy.

**Nonlinear isolator at microwave frequencies.** To realize the instantaneous Kerr effect at microwave frequencies, we used an antiparallel connection of two varactors as shown in Supplementary Fig. 1. The varactors are identical, have opposite polarities, and are biased with the same d.c. signal. Varactors are nonlinear elements and their effective capacitance for the RF signal can be described through a polynomial expansion as

$$C = C^{(0)} + C^{(1)}v_{\text{RF}} + C^{(2)}v_{\text{RF}}^2 + \dots \quad (21)$$

where the terms  $C^{(j)}$  with  $j=0,1,\dots$  depend only on the d.c. voltage, and  $v_{\text{RF}}$  is the radiofrequency (RF) signal in the time domain. Due to the antiparallel connection of the varactors, the RF signal at the two varactors has the same amplitude and opposite polarity; that is,  $v_{2,\text{RF}} = -v_{1,\text{RF}} = v_{\text{RB}}$  where  $v_{j,\text{RF}}$  is the RF voltage across the  $j$ th varactor, and  $v_{\text{RF}}$  is the RF voltage between terminals 1 and 2. Then, the capacitances of the two varactors are

$$\begin{aligned} C_1 &= C^{(0)} + C^{(1)}v_{\text{RF}} + C^{(2)}v_{\text{RF}}^2 + \dots \\ C_2 &= C^{(0)} - C^{(1)}v_{\text{RF}} + C^{(2)}v_{\text{RF}}^2 + \dots \end{aligned} \quad (22)$$

The total capacitance of the system is  $C = C_1 + C_2$ . Inserting equation (22) into this equality yields

$$C = 2C^{(0)} + 2C^{(2)}v_{\text{RF}}^2 + \dots \quad (23)$$

which can also be written as  $C = C_{\text{lin}}(1 + V_{\text{RF}}^2/V_0^2)$ , where  $C_{\text{lin}} = 2C^{(0)}$  and  $V_0 = \sqrt{C^{(0)}/C^{(2)}}$ . The total capacitance of the circuit thus has the same form as the permittivity of instantaneous Kerr nonlinear materials in optics.

**Data availability.** The data that support the plots within this paper and other findings of this study are available from the corresponding author upon reasonable request.

Received: 22 May 2017; Accepted: 15 January 2018;  
Published online: 8 February 2018

## References

- Pozar, D. M. *Microwave Engineering* 3rd edn (John Wiley & Sons, Hoboken, NY, 2005).
- Potter, R. J. Reciprocity in optics. *Rep. Prog. Phys.* **67**, 717–754 (2004).
- Kodera, T., Sounas, D. L. & Caloz, C. Magnetless nonreciprocal metamaterial (MNM) technology: application to microwave components. *IEEE Trans. Microw. Theory Techn.* **61**, 1030–1042 (2013).
- Wang, Z. et al. Gyrotropic response in the absence of a bias field. *Proc. Natl Acad. Sci. USA* **109**, 13194–13197 (2012).
- Sounas, D. L. & Alù, A. Non-reciprocal photonics based on time modulation. *Nat. Photon.* **11**, 774–783 (2017).
- Yu, Z. & Fan, S. Complete optical isolation created by indirect interband photonic transitions. *Nat. Photon.* **3**, 91–94 (2009).
- Lira, H., Yu, Z., Fan, S. & Lipson, M. Electrically driven nonreciprocity induced by interband photonic transition on a silicon chip. *Phys. Rev. Lett.* **109**, 033901 (2012).
- Wang, D.-W. et al. Optical diode made from a moving photonic crystal. *Phys. Rev. Lett.* **110**, 093901 (2013).
- Qin, S., Xu, Q. & Wang, Y. E. Nonreciprocal components with distributedly modulated capacitors. *IEEE Trans. Microw. Theory Techn.* **62**, 2260–2272 (2014).
- Sounas, D. L., Caloz, C. & Alù, A. Giant non-reciprocity at the subwavelength scale using angular momentum-biased metamaterials. *Nat. Commun.* **4**, 2407 (2013).
- Fleury, R., Sounas, D. L., Sieck, C. F., Haberman, M. R. & Alù, A. Sound isolation and giant linear nonreciprocity in a compact acoustic circulator. *Science* **343**, 516–519 (2014).
- Sounas, D. L. & Alù, A. Angular-momentum-biased nanorings to realize magnetic-free integrated optical isolation. *ACS Photon.* **1**, 198–204 (2014).

13. Estep, N. A., Sounas, D. L., Soric, J. & Alù, A. Magnetic-free non-reciprocity and isolation based on parametrically modulated coupled-resonator loops. *Nat. Phys.* **10**, 923–927 (2014).
14. Reiskarimian, N. & Krishnaswamy, H. Magnetic-free non-reciprocity based on staggered commutation. *Nat. Commun.* **7**, 11217 (2015).
15. Gallo, K., Assanto, G., Parameswaran, K. R. & Fejer, M. M. All-optical diode in a periodically poled lithium niobate waveguide. *Appl. Phys. Lett.* **79**, 314–316 (2001).
16. Zhou, H. et al. All-optical diodes based on photonic crystal molecules consisting of nonlinear defect pairs. *J. Appl. Phys.* **99**, 123111 (2006).
17. Shadrivov, I. V., Fedotov, V. A., Powell, D. A., Kivshar, Y. S. & Zheludev, N. I. Electromagnetic wave analogue of an electronic diode. *New J. Phys.* **13**, 033025 (2011).
18. Lepri, S. & Casati, G. Asymmetric wave propagation in nonlinear systems. *Phys. Rev. Lett.* **106**, 164101 (2011).
19. Anand, B. et al. Optical diode action from axially asymmetric nonlinearity in an all-carbon solid-state device. *Nano. Lett.* **13**, 5771–5776 (2013).
20. Peng, B. et al. Parity–time-symmetric whispering-gallery microcavities. *Nat. Phys.* **10**, 394–398 (2014).
21. Lin, X.-S., Yan, J.-H., Wu, L.-J. & Lan, S. High transmission contrast for single resonator based all-optical diodes with pump-assisting. *Opt. Express* **16**, 20949–20954 (2008).
22. Manipatruni, S., Robinson, J. T. & Lipson, M. Optical nonreciprocity in optomechanical structures. *Phys. Rev. Lett.* **102**, 213903 (2009).
23. Miroschnichenko, A. E., Brasselet, E. & Kivshar, Y. S. Reversible optical nonreciprocity in periodic structures with liquid crystals. *Appl. Phys. Lett.* **96**, 063302 (2010).
24. Roy, D. Few-photon optical diode. *Phys. Rev. B* **81**, 155117 (2010).
25. Zhukovsky, S. V. & Smirnov, A. G. All-optical diode action in asymmetric nonlinear photonic multilayers with perfect transmission resonances. *Phys. Rev. A* **83**, 023818 (2011).
26. Aleahmad, P., Khajavikhan, M., Christodoulides, D. & LiKamWa, P. Garnet-free optical circulators monolithically integrated on spatially modified iii–v quantum wells. Preprint at <https://arxiv.org/abs/1606.06949> (2016).
27. Fan, L. et al. An all-silicon passive optical diode. *Science* **335**, 447–450 (2012).
28. Fan, L. et al. Silicon optical diode with 40 dB nonreciprocal transmission. *Opt. Lett.* **38**, 1259–1261 (2013).
29. Xu, Y. & Miroschnichenko, A. E. Reconfigurable nonreciprocity with a nonlinear Fano diode. *Phys. Rev. B* **89**, 134306 (2014).
30. Yu, Y. et al. Nonreciprocal transmission in a nonlinear photonic-crystal Fano structure with broken symmetry. *Laser Photon. Rev.* **9**, 241–247 (2015).
31. Mahmoud, A. M., Davoyan, A. R. & Engheta, N. All-passive nonreciprocal metastructure. *Nat. Commun.* **6**, 8359 (2015).
32. Ding, W., Luk'yanchuk, B. & Qiu, C.-W. Ultrahigh-contrast-ratio silicon Fano diode. *Phys. Rev. A* **85**, 025806 (2012).
33. Shi, Y., Yu, Z. & Fan, S. Limitations of nonlinear optical isolators due to dynamic reciprocity. *Nat. Photon.* **9**, 388–392 (2015).
34. Sounas, D. L. & Alù, A. Time-reversal symmetry bounds on the electromagnetic response of asymmetric structures. *Phys. Rev. Lett.* **118**, 154302 (2017).
35. Grigoriev, V. & Biancalana, F. Nonreciprocal switching thresholds in coupled nonlinear microcavities. *Opt. Lett.* **36**, 2131–2133 (2011).
36. Little, B. E., Chu, S. T., Haus, H. A., Foresi, J. & Laine, J.-P. Microring resonator channel dropping filters. *J. Lightwave Technol.* **15**, 998–1005 (1997).
37. Haus, H. A. *Waves and Fields in Optoelectronics* (Prentice-Hall, Englewood Cliffs, NJ, 1984).
38. Suh, W., Wang, Z. & Fan, S. Temporal coupled-mode theory and the presence of non-orthogonal modes in lossless multimode cavities. *IEEE J. Quantum Electron.* **40**, 1511 (2004).

### Acknowledgements

This work was supported by the Air Force Office of Scientific Research with grant No. FA9550-17-1-0002, the Simons Foundation and the National Science Foundation.

### Author contributions

All authors contributed equally to this work, including development of the concept, design and execution of the experiment, and manuscript preparation.

### Competing interests

The authors declare no competing financial interests.

### Additional information

**Supplementary information** is available for this paper at <https://doi.org/10.1038/s41928-018-0025-0>.

**Reprints and permissions information** is available at [www.nature.com/reprints](http://www.nature.com/reprints).

**Correspondence and requests for materials** should be addressed to A.A.

**Publisher's note:** Springer Nature remains neutral with regard to jurisdictional claims in published maps and institutional affiliations.